

Electrically Tunable Surface Acoustic Wave Propagation at MHz Frequencies Based on Carbon Nanotube Thin-Film Transistors

Chen Shen, Shiheng Lu, Zhenhua Tian, Shujie Yang, Jorge A. Cardenas, Junfei Li, Xiuyuan Peng, Tony Jun Huang,* Aaron D. Franklin,* and Steven A. Cummer*

Surface acoustic waves (SAWs) that propagate on the surface of a solid at MHz frequencies are widely used in sensing, communication, and acoustic tweezers. However, their properties are difficult to be tuned electrically, and current devices suffer from complicated configurations, complicated tuning mechanisms, or small ranges of tunability. Here a structure featuring a thin-film transistor configuration is proposed to achieve electrically tunable SAW propagation based on conductivity tuning. When a DC gate voltage is applied, the on-site conductivity of the piezoelectric substrate is modulated, which leads to velocity and amplitude tuning of SAWs. The use of carbon nanotubes and crystalline nanocellulose as the channel and gate materials results in high tuning capacity and low gate voltage requirement. The tunability is manifested by a 2.5% phase velocity tuning and near 10 dB on/off switching of the signals. The proposed device holds the potential for the next generation SAW-based devices.

than their radiofrequency counterpart, SAW devices have been widely employed in wireless and adaptive communications.^[1,2] SAWs can interact with piezoelectric substrates on which they are propagating, and they find applications in sensing^[3,4] and analog signal processing.^[5] Using SAWs for quantum pumping of charge carriers has also been an active research topic.^[6,7] In recent years, SAW-based microfluidics begin to emerge as a new platform for particle and cell manipulation due to its label-free, high-throughput and bio-compatible properties.^[8–10] In all these applications, the ability to control SAW propagation, specifically the phase velocity and attenuation, adds additional degrees of freedom for improved performance of these functionalities.^[11–13]

1. Introduction

The investigation of surface acoustic waves (SAWs) dates back over a hundred years. As SAW wavelengths are much shorter

Many SAW devices use piezoelectric materials as their substrates, which convert electrical excitation to mechanical vibrations and vice versa when integrated with interdigital transducers (IDTs). The electrical and mechanical properties of the substrate or the structures patterned on its surface affect the SAWs propagating on the substrate based on piezoelectric and electromechanical coupling effects.^[14] These effects have been employed to control the propagation of SAWs in an on-chip manner. For example, surface phononic crystals and non-linear nanoelectromechanical resonators that operate in the MHz regime can interact with elastic waves and tune their propagation characteristics.^[15–19] This approach, however, requires judiciously designed architectures that are typically in the wavelength scale, which poses challenges on reliable fabrication. Moreover, these devices may not be compatible with some sensing and biomedical applications because of the delicate components, leading to difficulties in the integration of the devices. As an alternative means, devices that can control the electrical properties of the substrate have also been proposed for SAW modulation. Specifically, SAW devices featuring a gate-voltage tuning mechanism emerge as a promising avenue as they are directly transferable to on-chip devices for various applications.^[20–23] Field-effect transistors, the ubiquitous three-terminal semiconductor devices that allow their channel conductivity to be tuned by orders of magnitude by applying a gate voltage, offers a promising path towards the electrical tuning of SAW propagation in a controllable manner. Previously reported devices, however, suffer from high gate voltage requirements, limited tunability, complicated heterostructures


Prof. C. Shen, S. Lu, Dr. J. A. Cardenas, Dr. J. Li, X. Peng,
Prof. A. D. Franklin, Prof. S. A. Cummer
Department of Electrical and Computer Engineering
Duke University
Durham, NC 27708, USA
E-mail: aaron.franklin@duke.edu; cummer@duke.edu

Prof. C. Shen
Department of Mechanical Engineering
Rowan University
Glassboro, NJ 08028, USA

Prof. Z. Tian, S. Yang, Prof. T. J. Huang
Department of Mechanical Engineering and Materials Science
Duke University
Durham, NC 27708, USA
E-mail: tony.huang@duke.edu

Prof. Z. Tian
Department of Aerospace Engineering
Mississippi State University
Starkville, MS 39762, USA

Prof. A. D. Franklin
Department of Chemistry
Duke University
Durham, NC 27708, USA

 The ORCID identification number(s) for the author(s) of this article can be found under <https://doi.org/10.1002/adfm.202010744>.

DOI: 10.1002/adfm.202010744

and cumbersome fabrication processes which significantly hamper their real-world applications.

In this work, we demonstrate electrically tunable SAW propagation on a lithium niobate (LiNbO₃) substrate at MHz frequencies. We use carbon nanotube thin-film transistors (CNT-TFTs) printed directly on the substrate to tune the surface conductivity. The use of printing technologies has demonstrated its potential in manufacturing of thin-film devices with low cost and high material versatility.^[24] Semiconducting CNTs are selected as the channel material due to its semiconducting nature and high electron mobility which together offer a range of sheet resistance suitable for SAW modulation. In addition, CNTs are compatible with low-cost solution-based processing methods. To reduce the gate voltage requirement, we employ an ionic material (crystalline nanocellulose, CNC) as the gate dielectric. The device features low gate voltage (± 1 V) and large dynamic range, which results in a high tuning capacity evidenced by a 2.5% phase velocity tuning range, a dramatic increase as compared with previous devices that use low gate voltage.^[14, 23] Near 10 dB switching on and off the signals is also demonstrated by a propagation distance of 20 wavelengths. The gate-controllable SAW modulation can be used in a number of applications including sensing, communication, and SAW-based acoustic tweezers.

2. Results

2.1. Mechanism and Design of Tunable SAW Propagation

Figure 1 shows a schematic diagram of the proposed tunable SAW chip. It consists of a pair of IDTs on a YX-128° LiNbO₃ substrate (SAW velocity 3980 m s⁻¹) for the actuation and sensing of SAWs. The width of the IDT fingers and the gap between adjacent IDT fingers are both 12.5 μ m, corresponding to an operation frequency of 80 MHz. A CNT-TFT is fabricated along the propagation path of SAWs. An atomically thin CNT layer is printed on the substrate as the channel, whose conductivity can

be modulated by on-site electric fields. As the thickness of the CNT layer is much thinner than the wavelength, the velocity change and attenuation induced by the conductivity modulation can be expressed as:^[25]

$$\frac{\Delta v}{v_{oc}} = \frac{K_{eff}^2}{2} \frac{1}{1 + (\sigma_d / \sigma_m)^2} \quad (1)$$

$$\Gamma = k \frac{K_{eff}^2}{2} \frac{\sigma_d / \sigma_m}{1 + (\sigma_d / \sigma_m)^2} \quad (2)$$

where v_{oc} is the phase velocity when the CNT layer is fully depleted, and K_{eff}^2 is the effective electromechanical coupling coefficient that is 5.6% for YX-128° LiNbO₃ substrates. σ_d is the conductivity of the CNT layer, σ_m is the characteristic conductivity at which maximum attenuation occurs, and k is the wave vector of the SAW without modulation.

Based on the theoretical model, the phase velocity and attenuation of the SAW at a given substrate conductivity can be calculated. Numerical simulations based on commercial finite element package COMSOL are also performed to validate the model^[25] (Figure S1, Supporting Information). The results are shown in Figure 2, where excellent agreement can be found between the theory and the simulation. Here we use sheet resistance as a measure of the electrical properties of the channel, which provides a more accurate means for characterization (Figure S2, Supporting Information). The sheet resistance can be related to the conductivity by $R_s = 1/\sigma t$, where t is the thickness of the channel and is 20 nm in this study. By controlling the conductivity of the channel, the phase velocity can be modulated. The maximum tuning capacity of phase velocity is 2.8%, which is dictated by the effective electromechanical coupling coefficient and is independent of the modulation strategy.

To achieve the required conductivity modulation, here we implement a micromachined TFT using a top-gate configuration. TFTs can effectively modulate the conductivity of the channel by properly choosing the semiconducting material.

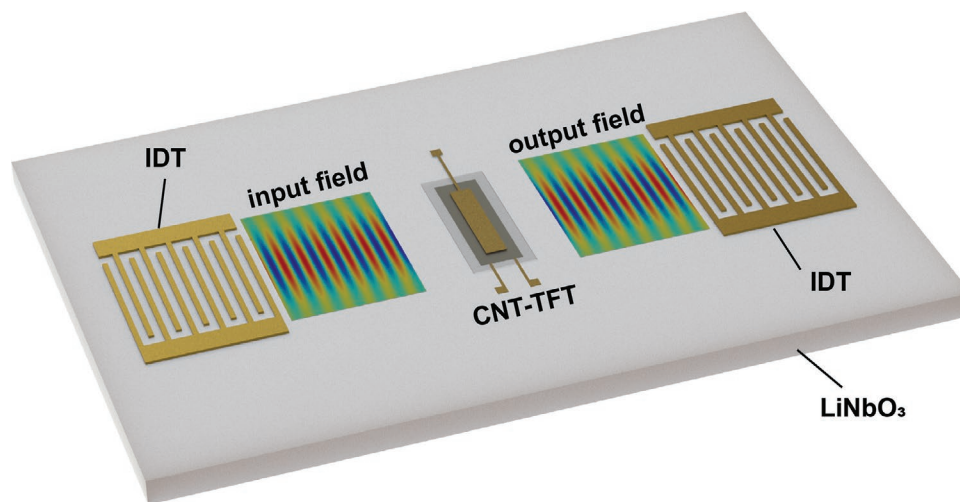


Figure 1. Schematic of a tunable SAW chip based on a top-contact CNT-TFT. Using a transistor configuration, the SAWs transmitting across the channel will be modulated by applying a gate voltage, leading to tunable output fields.

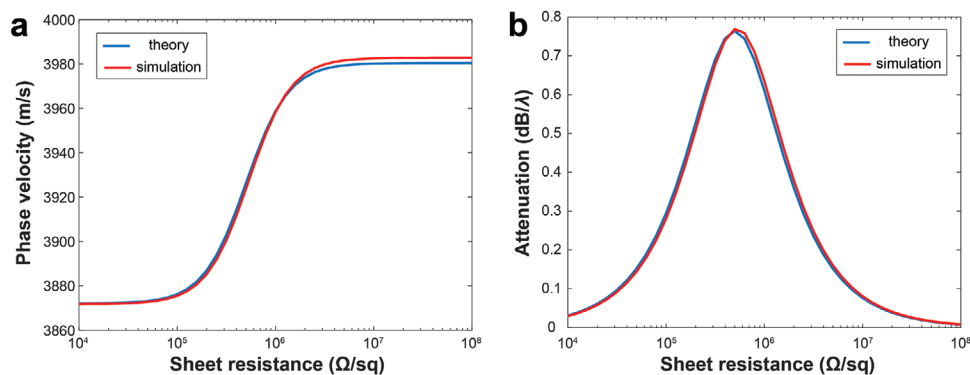


Figure 2. Calculated and simulated tuning of the SAW based on conductivity modulation. a) Phase velocity. b) Attenuation.

The CNTs we used here have shown promising capabilities of tuning the conductivity across an order of ten to the fourth, which is sufficient for the modulation of SAWs. The insulating material itself (i.e., the dielectric in between the channel and the top gate), on the other hand, will also affect the SAW propagation on the substrate. Its effect, however, is rarely studied because of the complexities. Here we use full-wave numerical simulations to study the tuning of the SAWs where both the electrical and mechanical properties of the dielectric layer are considered. The dielectric material is modeled based on a complex dielectric permittivity which is written as:

$$\epsilon_r = \epsilon - i\sigma_d / \omega \epsilon_0 \quad (3)$$

where ϵ and σ_d are the permittivity and conductivity of the dielectric layer, ω is the angular frequency. As there exists a gate electrode on top, the conductivity of the dielectric layer cannot exceed a certain value so that sufficient insulation effect can be provided. **Figure 3a** exhibits the phase velocity tuning of the SAWs with respect to different conductivity. Results indicate that the tuning effect is absent above a certain threshold. As standard dielectric materials generally have a very small conductivity, this requirement can be easily met. Another important factor that affects the SAW propagation is the permittivity ϵ . **Figure 3b** shows the relationship of SAW velocity tuning with respect to the permittivity of the dielectric layer. It can be seen that the tuning capacity increases with the thickness of the dielectric layer. The required thickness is also smaller for

lower permittivity to achieve the same velocity tuning range. Although for high permittivity materials, one can increase the thickness to achieve better tuning effect, a thick dielectric layer can overwhelm the SAWs propagation on the substrate through the mechanical effect. For example, when a material loss of $\tan\delta = 0.1$ is considered, the attenuation of SAWs caused by the mechanical effect can increase dramatically when a thicker dielectric layer is used, as indicated by **Figure 3c**. This implies that to obtain high tuning capacity, dielectric materials with smaller permittivity is preferred as more attenuation is accompanied with larger thickness.

We aim to achieve high tuning capacity of SAWs with low gate voltage requirements in this study (**Figure S3**, Supporting Information). While there are many low-impedance dielectric materials that can be processed into micrometer-thick thin-films via low-cost solution-based methods, the resultant TFTs usually require high gate voltage to achieve a decent current modulation.^[26,27] The use of high ϵ dielectric materials, on the other hand, is a well-established strategy to reduce the operating voltage,^[28] yet it is suggested in **Figure 3b** that a low-permittivity dielectric layer gives weak modulation in phase velocity. Ionic dielectric materials, which offer gate capacitance determined by the electron double layers instead of their thicknesses, are also commonly used to realize thin-film transistors with low operating voltages.^[29–31] A major limitation of ionically gated transistors is that their response time is strongly related to its ionic conductivity, which is usually much longer compared to the dielectrically gated ones.^[32,33] This could limit their applications

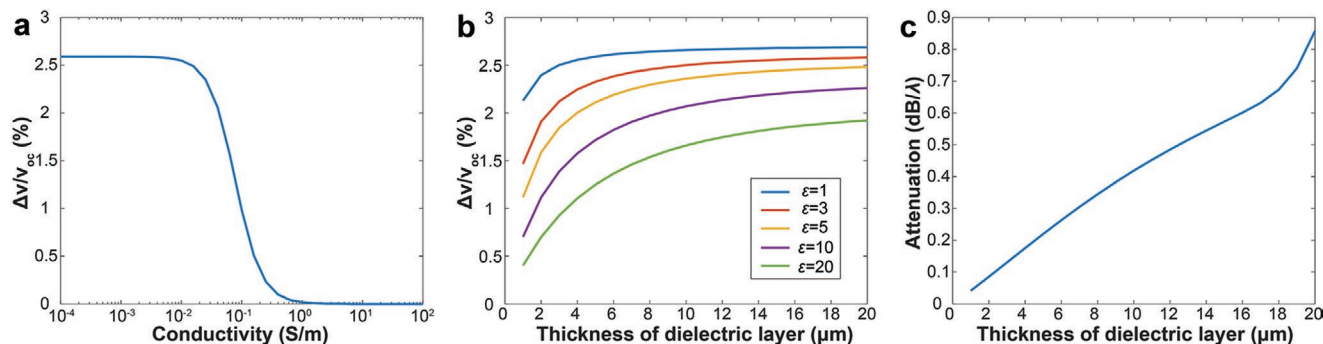


Figure 3. SAW modulation with different dielectric layer properties from numerical simulations. a) Dependence of tuning capacity on the conductivity of the dielectric layer. b) Effect of dielectric constant on the tuning capacity. c) Attenuation caused by the mechanical effect of the dielectric layer.

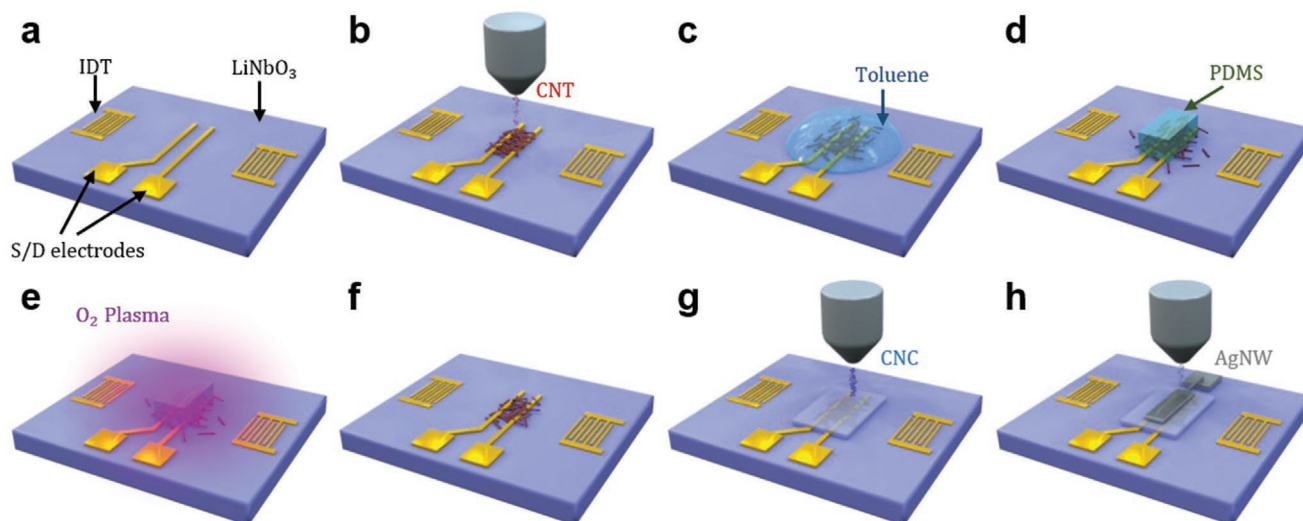


Figure 4. Schematic illustrations of the fabrication process flow. a) Patterning and depositing the source and drain electrodes using optical lithography and e-beam evaporation; b) carbon nanotube (CNT) thin-film channel printing; c) toluene rinsing to remove the residual polymers, the CNT film would spread out during this process; d) covering the channel with PDMS; e) etching of the unwanted CNTs using oxygen plasma; f) unmasking the channel; g) CNC dielectric layer printing; h) silver nanowire (AgNW) gate electrode printing.

that require dynamic or fast response. Nevertheless, ionic dielectrics still exhibit their potential for applications such as non-hazardous gas sensing and reconfigurable SAW-based particle and droplet manipulation.^[34] In this work, we employ CNC as the gate material as it is reported to yield small permittivity at MHz frequencies.^[35]

2.2. Fabrication and Characterization of the CNT-TFT

Based on the design strategy outlined in the previous section, CNT-TFTs are fabricated on lithium niobate (LiNbO₃) substrates, with detailed illustrations of the fabrication process flow shown in **Figure 4** and the experimental section. The CNT-TFT is positioned at the center of the substrate and is about 2 mm away from the IDTs to avoid possible contamination as they are fabricated separately. In brief, the source and drain electrodes were patterned and deposited using optical lithography and e-beam evaporation, and the CNT thin-film channels were aerosol-jet-printed. After printing the channels, the samples were rinsed with toluene to get rid of the polymer surfactants and thus enhance the channel mobility. It is worth noting that the CNTs would spread out on LiNbO₃ substrates during the rinsing step, and an additional patterning step was carried out to ensure that the channels are well defined. The channel areas were protected by pieces of polydimethylsiloxane (PDMS), with the unwanted CNTs etched using oxygen plasma. After removing the PDMS, CNC and silver nanowires (AgNW) were aerosol-jet-printed as the gate dielectric layers and the gate electrodes, respectively.

The morphology of the printed CNT-TFTs are given in **Figure 5**. An optical image and a schematic diagram, shown in **Figures 5a** and **5b**, respectively, demonstrate the overall device structure, whereas the scanning electron microscope (SEM) images presented in **Figure 5c–f** provide a detailed film morphology illustration of various device layers. The thickness of

the CNC layer is around 5 μm, and the thickness of the AgNW layer is comparable to the roughness of the underlying CNC film. The SEM imaging and the profilometry measurement (**Figure S4**, Supporting Information) are in good agreement with each other. The ionic conductivity of CNC was estimated by fitting the impedance spectroscopy data with a simplified model^[36] (**Figure S4**, Supporting Information). The combination of the extracted ionic conductivity and the film thickness suggests that the ions within the CNC layer offer a sheet resistance at the order of 10⁸ Ω sq⁻¹, which is roughly 10× higher compared to the upper bound of the dynamic range presented in **Figure 1**. This indicates that the coupling between the ions within the CNC and the SAW is unlikely to have any impact on either the phase or the amplitude of the signal.

2.3. Modulation of SAWs with the Tunable Chip

The fabricated device is further tested on a probe station. The experimental setup is shown in **Figure 6a**. The total length of the channel which SAWs propagate through is around 1 mm, which corresponds to 20 wavelengths. A voltage is applied on the gate electrode and is slowly varying from -1V to 1V as the CNC needs time to be fully polarized for operation. The source and drain electrodes are also connected to the probe station to monitor the conductivity change across the channel (**Figure S5**, Supporting Information). At the mean time, the source IDT is excited using a function generator and the signals are recorded at the receiving IDT. In the measurements, pulsed signals are used and the signals are averaged to reduce noises.

The transfer and subthreshold characteristics of the CNT-TFT is plotted **Figure 6b**, where a modulation of almost four orders of magnitude is observed in terms of the channel sheet resistance. The measured sheet resistance is then plugged into **Equations (1)** and **(2)** to predict the corresponding phase velocity and attenuation change according to the conductivity

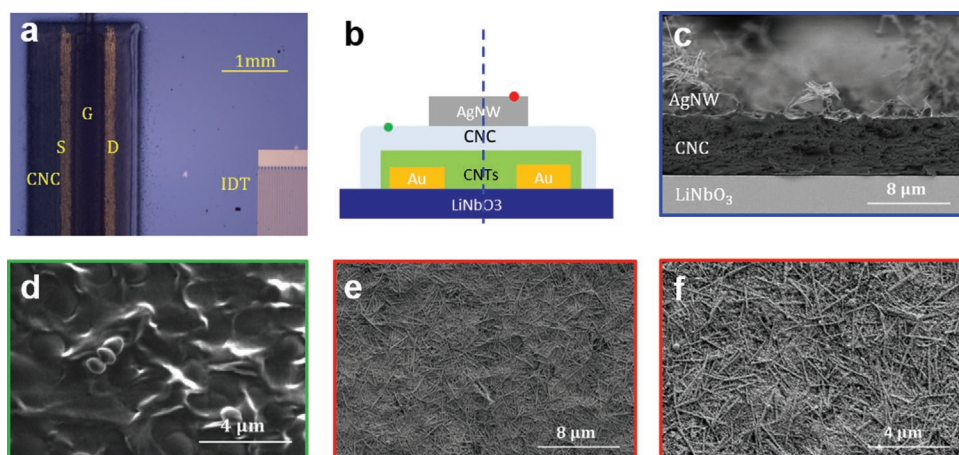


Figure 5. Microscopic characterizations of printed CNT-TFTs. a) An optical image of a CNT-TFT printed on a LiNbO₃ substrate. b) A schematic diagram illustrating the cross section of a printed CNT-TFT and locations for SEM imaging. c) A SEM image of the CNT-TFT from cross-sectional view. Top-view SEM images of d) the printed CNC film and e,f) the printed AgNW/CNC stack.

modulation. The results are compared with those obtained from measurements in Figure 6c,d. Good agreement can be found between the theoretical calculations and experimental results. The measured results also show a larger dynamic range and a smaller amplitude modulation compared with the theory. This could be attributed to the nonuniformity of the channel as different components of a CNT network exhibit different conductivity. For example, the resistivity of a junction between two CNTs is much higher than the resistivity within the same tube.^[37] The conductivity of these components enter and leave the dynamic range under different gate bias, which causes the widening of the effective dynamic range. Thanks to the semiconducting nature of the CNTs and the relatively low permittivity of the CNC, the velocity can be tuned by up to 2.5%, which approaches the theoretical value of 2.8% for the used LiNbO₃ substrates. In addition, near 10 dB on/off ratio of SAW signal strength is achieved across the transition region, which is again enabled by applying a small gate voltage. The maximum attenuation is around 0.5 dB per wavelength, which is smaller than the theoretical prediction. This could be caused by the nonuniformity of the channel and the dielectric layer, and the different mechanical effects between interfacial layers when the device is switched on or off.^[38] Nevertheless, the results mark a meaningful tunability aimed at SAW-based applications in sensing and acoustic tweezers.

3. Conclusions

In this study, we demonstrated SAW modulation using conductivity tuning on a lithium niobate substrate. Aerosol-jet-printed CNT-TFTs are used to achieve the required conductivity tuning. A numerical approach based on finite element analysis is used to predict the behavior of the device and help determine the optimal parameters. The TFTs are directly fabricated by aerosol jet printing on the substrate with small footprints. Measurements show that the sheet resistance can be tuned by a factor of 10⁴, which fully covers the transition region and leads to efficient SAW modulation. A phase velocity tuning effect as much as 2.5% is observed, which surpasses previous devices using similar mechanisms.^[20–23] On-off amplitude switching of the signals is also demonstrated in the proposed structure by tuning the SAW attenuation.

The device, which features CNT as the channel material and CNC as the gate material, exhibits several unique advantages. First, it enables large conductivity tuning, which is crucial for the realization of tunable SAW devices. Second, the device has simple structural configuration. Most components can be directly printed on the substrate, which is much more convenient than previous proposals using heterogeneous structures or two-dimensional electron gases. Thanks to the

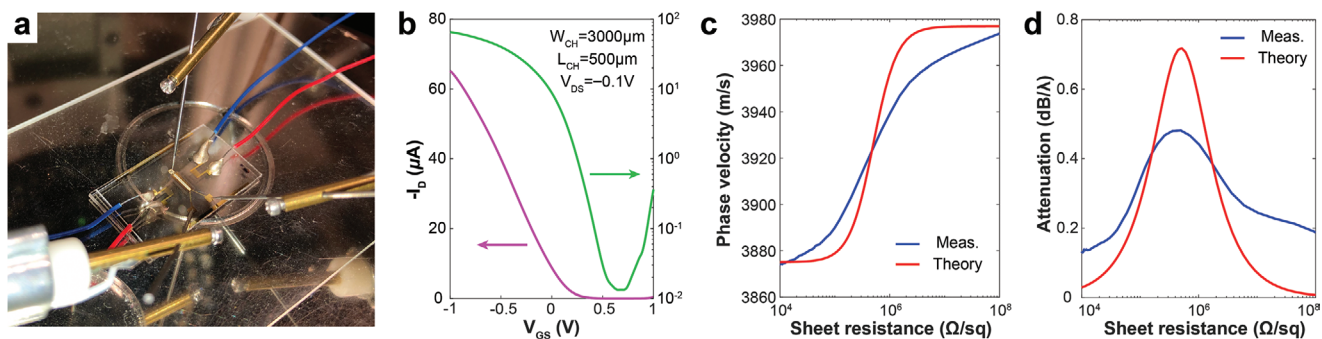


Figure 6. Experimental demonstration of SAW modulation. a) Experimental setup on a probe station. b) Transfer (magenta) and subthreshold (green) characteristics of a CNT-TFT printed on LiNbO₃ substrate. c) SAW velocity modulation. d) SAW amplitude modulation.

semiconducting nature of CNTs, larger velocity modulation is achieved compared to the use of other channel materials such as graphene. The low gate voltage requirement also makes it possible to transfer the device to other applications including sensing, communication, and SAW-based particle manipulation that use a voltage as the input/output. It is hoped that the proposed device can be used toward a number of applications that require tunable acoustic components.

4. Experimental Section

Numerical Simulations: Numerical results were obtained through finite element method using commercial solver COMSOL Multiphysics 5.4. The Solid Mechanics module containing piezoelectric materials and the Electrostatics module were used so that piezoelectric coupling and electromechanical coupling were taken into consideration. The phase speed of the SAWs depending on the sheet resistance of the channel was acquired by calculating the eigenfrequency of a period of the structure. The corresponding attenuation caused by the conductivity modulation was extracted from the imaginary part of the eigenfrequency.

Source and Drain Electrodes Fabrication: The patterning of the source and drain electrodes was done via a Karl Suss MA6/BA6 mask aligner. S1813 was selected as the photoresist, and the exposure took 11 s using CI (365 nm) with a dose of 120 J cm^{-2} . 5-nm Ti/ 50-nm Au was deposited as the source and drain electrodes using an E-beam evaporator (Kurt Lesker PVD 75). The lift-off process was performed by immersing the sample in $50 \text{ }^\circ\text{C}$ acetone for 1 h, sonicating the sample in acetone for 10 s, rinsing with acetone, isopropyl alcohol, and deionized water, followed by a nitrogen blow-drying.

Substrate Functionalization: After the lift-off steps, the samples underwent a 3-min 100 W oxygen plasma treatment using an Emitech K-1050X plasma asher, a 5-min immersion in PLL solution (0.1 mg mL^{-1} , Sigma-Aldrich), DI water rinsing, and nitrogen blow-drying. The functionalization steps enhanced the substrate adhesion of carbon nanotubes.

CNT Channel Printing: The CNT channels were printed using an Optomec AJ300 aerosol jet printer with a $150\text{-}\mu\text{m}$ nozzle. Commercial CNT ink (0.1 mg/mL , IsoSol-S100, NanoIntegris), was mixed with toluene by a volume ratio of 1:4, and 1000 mL of the as-prepared CNT ink was loaded into the printer. The sheath flow rate, the carrier gas flow rate, and the ultrasonic current, were set to be 40 sccm, 23 sccm, and 330 mA, respectively. The platen moved at a speed of 4 mm s^{-1} , and 1 pass of CNTs was printed as the channel. Once the CNT printing was finished, the samples were rinsed in toluene for 30 s to remove the polymer residue and to increase the channel mobility. After that, the samples underwent a 1-min treatment in 100 W oxygen plasma to etch the extra CNTs while the channel regions were covered and protected by PDMS films.

CNC Printing and AgNW Printing: the CNC dielectric layers and the AgNW electrodes were prepared and printed according to the aerosol jet printing protocol described in the reference. The CNC^[39] and AgNW^[40] inks were both printed using an Optomec AJ300 aerosol jet printer. While a $300 \text{ }\mu\text{m}$ nozzle was used for CNC printing, AgNW electrodes were printed using a $200 \text{ }\mu\text{m}$ nozzle with smallest size being around $100 \text{ }\mu\text{m}$. Such a printing resolution is expected to ensure the quality of devices aiming at SAWs at MHz frequencies.

Microscopic Imaging and Profilometry Characterizations: Zeiss Axio Compound Microscope, together with the incorporated digital camera, was used to take the optical images. An Apreo S Scanning electron microscopy (SEM) from ThermoFisher Scientific was selected to perform the SEM imaging. The film thicknesses of printed CNC and AgNW were measured using a Bruker Dektak 150 profilometer.

SAW Signals Acquisition: The SAW signals acquisition was done by exciting the source IDTs and directly measuring the signals from the receiving IDTs. A function generator (model DG4202) was used to generate the input pulsed signals at a central frequency of 80 MHz. The

transmitted signals were captured by an oscilloscope (model DS1074) and were averaged out of 128 measurements to reduce noise. At the mean time, a slowly varying gate voltage (0.5 V min^{-1}) was applied from the probe station. This change was slow enough such that the gate voltage could be assumed constant when the signals were measured. The corresponding phase speeds at different gate voltages were then obtained by comparing the SAW signals acquired at different times (Figure S5, Supporting Information).

Supporting Information

Supporting Information is available from the Wiley Online Library or from the author.

Acknowledgements

C.S., S.L., and Z.T. contributed equally to this work. This work was performed in part at the Duke University Shared Materials Instrumentation Facility (SMIF), a member of the North Carolina Research Triangle Nanotechnology Network (RTNN), which is supported by the National Science Foundation (award number ECCS-2025064) as part of the National Nanotechnology Coordinated Infrastructure (NNCI). This work was supported by National Science Foundation (Grant Nos. EFMA-1641084 and ECCS-1807601), the Department of Defense Congressionally Directed Medical Research Program (CDMRP) (award number W81XWH-17-2-0045), and the National Institutes of Health (Grant Nos. R01GM132603, R33CA223908, R01GM127714, and 1R01HL146849).

Conflict of Interest

T.J.H. has co-founded a start-up company, Ascent Bio-Nano Technologies Inc., to commercialize technologies involving acoustofluidics and acoustic tweezers.

Data Availability Statement

Research data are not shared.

Keywords

aerosol jet printing, carbon nanotubes, nanocellulose, surface acoustic waves, thin-film transistors

Received: December 14, 2020

Revised: January 19, 2021

Published online: February 25, 2021

- [1] K.-Y. Hashimoto, *Surface Acoustic Wave Devices in Telecommunications*, Springer, New York 2000.
- [2] A. Stern, D. K. Efimkin, V. Galitski, Z. Fisk, J. Xia, *Phys. Rev. Lett.* **2016**, *116*, 166603.
- [3] K. Länge, B. E. Rapp, M. Rapp, *Anal. Bioanal. Chem.* **2008**, *391*, 1509.
- [4] S. Okuda, T. Ono, Y. Kanai, T. Ikuta, M. Shimatani, S. Ogawa, K. Maehashi, K. Inoue, K. Matsumoto, *ACS Sensors* **2018**, *3*, 200.
- [5] D. Morgan, *Surface Acoustic Wave Filters: With Applications to Electronic Communications and Signal Processing*, Academic Press, San Diego, CA 2010.
- [6] C. Rocke, S. Zimmermann, A. Wixforth, J. P. Kotthaus, G. Böhm, G. Weimann, *Phys. Rev. Lett.* **1997**, *78*, 4099.
- [7] O. Couto, S. Lazić, F. Iikawa, J. Stotz, U. Jahn, R. Hey, P. Santos, *Nat. Photonics* **2009**, *3*, 645.

- [8] A. Ozcelik, J. Rufo, F. Guo, Y. Gu, P. Li, J. Lata, T. J. Huang, *Nat. Methods* **2018**, *15*, 1021.
- [9] L. Ren, S. Yang, P. Zhang, Z. Qu, Z. Mao, P.-H. Huang, Y. Chen, M. Wu, L. Wang, P. Li, T. J. Huang, *Small* **2018**, *14*, 1801996.
- [10] A. Huang, H. Liu, O. Manor, P. Liu, J. Friend, *Adv. Mater.* **2020**, *32*, 1907516.
- [11] R. Manenti, A. F. Kockum, A. Patterson, T. Behrle, J. Rahamim, G. Tancredi, F. Nori, P. J. Leek, *Nat. Commun.* **2017**, *8*, 975.
- [12] K. J. Satzinger, Y. Zhong, H.-S. Chang, G. A. Peairs, A. Bienfait, M.-H. Chou, A. Cleland, C. R. Conner, É. Dumur, J. Grebel, I. Gutierrez, B. H. November, R. G. Povey, S. J. Whiteley, D. D. Awschalom, D. I. Schuster, A. N. Cleland, *Nature* **2018**, *563*, 661.
- [13] A. Palermo, Y. Wang, P. Celli, C. Daraio, *Phys. Rev. Appl.* **2019**, *11*, 044057.
- [14] A. Wixforth, J. Scriba, M. Wassermeier, J. P. Kotthaus, G. Weimann, W. Schlapp, *Phys. Rev. B* **1989**, *40*, 7874.
- [15] S.-Y. Yu, X.-C. Sun, X. Ni, Q. Wang, X.-J. Yan, C. He, X.-P. Liu, L. Feng, M.-H. Lu, Y.-F. Chen, *Nat. Mater.* **2016**, *15*, 1243.
- [16] B. Ash, S. Worsfold, P. Vukusic, G. Nash, *Nat. Commun.* **2017**, *8*, 174.
- [17] J. Cha, C. Daraio, *Nat. Nanotechnol.* **2018**, *13*, 1016.
- [18] M. Yan, J. Lu, F. Li, W. Deng, X. Huang, J. Ma, Z. Liu, *Nat. Mater.* **2018**, *17*, 993.
- [19] L. Shao, W. Mao, S. Maity, N. Sinclair, Y. Hu, L. Yang, M. Lončar, *Nat. Electron.* **2020**, *3*, 267.
- [20] J. Pedros, F. Calle, R. Cuerdo, J. Grajal, Z. Bougrioua, *Appl. Phys. Lett.* **2010**, *96*, 123505.
- [21] R. Li, P. I. Reyes, S. Ragavendiran, H. Shen, Y. Lu, *Appl. Phys. Lett.* **2015**, *107*, 073504.
- [22] R. Li, G. Li, W.-C. Hong, P. I. Reyes, K. Tang, K. Yang, S.-Y. Wang, H. Ye, Y. Li, L. Zhang, K. Kisslinger, Y. Lu, *Smart Mater. Struct.* **2018**, *27*, 085025.
- [23] L. Bandhu, G. R. Nash, *Nano Res.* **2016**, *9*, 685.
- [24] S. H. Kim, K. Hong, W. Xie, K. H. Lee, S. Zhang, T. P. Lodge, C. D. Frisbie, *Adv. Mater.* **2013**, *25*, 1822.
- [25] P. Zheng, D. W. Greve, I. J. Oppenheim, *IEEE Trans. Ultrason., Ferroelectr., Freq. Control* **2013**, *60*, 579.
- [26] C. Cao, J. B. Andrews, A. D. Franklin, *Adv. Electron. Mater.* **2017**, *3*, 1700057.
- [27] S. Lu, J. A. Cardenas, R. Worsley, N. X. Williams, J. B. Andrews, C. Casiraghi, A. D. Franklin, *ACS Nano* **2019**, *13*, 11263.
- [28] P. H. Lau, K. Takei, C. Wang, Y. Ju, J. Kim, Z. Yu, T. Takahashi, G. Cho, A. Javey, *Nano Lett.* **2013**, *13*, 3864.
- [29] M. Ha, Y. Xia, A. A. Green, W. Zhang, M. J. Renn, C. H. Kim, M. C. Hersam, C. D. Frisbie, *ACS Nano* **2010**, *4*, 4388.
- [30] M. D. Ferro, N. A. Melosh, *Adv. Funct. Mater.* **2018**, *28*, 1704335.
- [31] S. Lu, A. D. Franklin, *Nanoscale* **2020**, *12*, 23371.
- [32] J. H. Cho, J. Lee, Y. He, B. Kim, T. P. Lodge, C. D. Frisbie, *Adv. Mater.* **2008**, *20*, 686.
- [33] X. Wu, A. Surendran, J. Ko, O. Filonik, E. M. Herzig, P. Müller-Buschbaum, W. L. Leong, *Adv. Mater.* **2019**, *31*, 1805544.
- [34] S. P. Zhang, J. Lata, C. Chen, J. Mai, F. Guo, Z. Tian, L. Ren, Z. Mao, P.-H. Huang, P. Li, S. Yang, T. J. Huang, *Nat. Commun.* **2018**, *9*, 1.
- [35] D. Le Bras, M. Strømme, A. Mihranyan, *J. Phys. Chem. B* **2015**, *119*, 5911.
- [36] Z. Zou, J. Kai, M. J. Rust, J. Han, C. H. Ahn, *Sens. Actuators, A* **2007**, *136*, 518.
- [37] A. Znidarsic, A. Kaskela, P. Laiho, M. Gaberscek, Y. Ohno, A. G. Nasibulin, E. I. Kauppinen, A. Hassanien, *J. Phys. Chem. C* **2013**, *117*, 13324.
- [38] J. Devkota, K.-J. Kim, P. R. Ohodnicki, J. T. Culp, D. W. Greve, J. W. Lekse, *Nanoscale* **2018**, *10*, 8075.
- [39] N. X. Williams, G. Bullard, N. Brooke, M. J. Therien, A. D. Franklin, *arXiv:2009.10225*, **2020**.
- [40] I. E. Stewart, M. J. Kim, B. J. Wiley, *ACS Appl. Mater. Interfaces* **2017**, *9*, 1870.